Dzyaloshinskii-Moriya Interaction and Spiral Order in Spin-orbit Coupled Optical Lattices

Ming Gong[1], Yinyin Qian[1], V.W. Scarola[2], and Chuanwei Zhang[1,3*]
[1]*Department of Physics and Astronomy, Washington State University, Pullman, WA, 99164 USA*
[2]*Department of Physics, Virginia Tech, Blacksburg, Virginia 24061 USA*
[3]*Department of Physics, the University of Texas at Dallas, Richardson, Texas, 75080 USA*

We show that the recent experimental realization of spin-orbit coupling in ultracold atomic gases can be used to study different types of spiral order and resulting multiferroic effects. Spin-orbit coupling in optical lattices can give rise to the Dzyaloshinskii-Moriya (DM) spin interaction which is essential for spin spiral order. We derive an effective spin model in the deep Mott insulator region at half filling, and demonstrate that the DM interaction in optical lattices can be made extremely strong with realistic experimental parameters. The rich phase diagrams of the effective spin model for fermion and bosons are obtained via classical Monte Carlo simulations.

PACS numbers: 03.75Ss, 74.20.-z, 03.75.Lm

The interplay between ferroelectric and ferromagnetic order in complex multiferroic materials presents a set of compelling fundamental condensed matter physics problems with potential multifunctional device applications [1]. Ferroelectric and ferromagnetic order compete and normally cannot exist simultaneously in conventional materials. Coexistence of these orders often relies on strong correlation. In some strongly correlated systems, such as the perovskite transition metal oxides [2–7], these two phenomena can occur simultaneously. Construction and design of high-T_c magnetic ferroelectrics is still an open and active area of research [8]. These and other complex solids incorporate different types of interactions, including electron-electron interactions, electron-phonon interactions, spin-orbit (SO) couplings, lattice defects, and disorder, making the determination of multiferroic mechanisms a remarkable challenge for most materials. Due to the inherent complexity of the different interactions involved, the underlying mechanism for the emergence of multiferroic behavior is not fully clear [9, 10]. An unbiased and direct method to explore multiferroic behavior (e.g., dynamics, critical exponents, the impact of controlled disorder, etc.) in an ideal setting is thus highly appealing.

The realization of a superfluid to Mott insulator transition of ultracold atoms in optical lattices [11] opened fascinating prospects [12] for the emulation of a large variety of novel magnetic states and other strongly correlated phases found in solids. In optical lattices different types of interactions can in principle be independently tuned and controlled, thus providing an ideal platform for the emulation of quantum phases. This platform can offer great insight into the physics of complex solids that incorporate strong correlation. As a result, possible magnetic phase diagrams have been explored in the optical lattice setting [13–15]. For instance, it has been shown [13, 14] that the effective Hamiltonian of spin-1/2 atoms in optical lattices is the XXZ Heisenberg model in the deep Mott insulator regime. On the experimental side, superexchange interactions between two neighboring sites have already been demonstrated [16] and quantum simulation of frustrated classical magnetism in triangle optical lattices has also been realized [17]. These experimental achievements mark the first steps towards the quantum simulation of possible magnetic phase transitions in optical lattices.

In this letter, we show that the power of optical lattice systems to emulate magnetism can be combined with recent experimental developments [18–21] realizing SO coupling to emulate multiferroic behavior. Recently, SO coupled optical lattices have been shown to possess flat energy band [22], and important experimental progress [23] has been made for observing the single particle band dispersion (including the flat band) in SO coupled optical lattices. The main findings of this work are the following: (I) We derive the effective Hamiltonian for spin-1/2 fermions and bosons in optical lattices in the large interaction limit. We show that SO coupling leads to an effective in-plane Dzyaloshinskii-Moriya (DM) term, an essential ingredient in models of spiral order and multiferroic effects in general. We estimate that the DM term is of the same order as the Heisenberg coupling constant, J. (II) We study the phase diagram of the effective spin model using classical Monte Carlo (MC). We find that competing types of spiral order depend strongly on the SO coupling strength and effective Zeeman field. (III) We find that the critical temperature for the spiral order can be made rather high, $\sim J$. Thus, if magnetic quantum phase transitions can be emulated in optical lattices, then spiral order and multiferroics can also be realized in the same setup with the inclusion of SO coupling.

Effective Hamiltonian: We consider spin-1/2 ultracold atoms loaded into a two-dimensional (2D) square optical lattice. We restrict ourselves to the deep Mott insulator regime where the charge/mass degree of freedom is frozen while the spin degree of freedom remains active. Here the atomic hyperfine levels map onto effective spin states. The scattering length between the atoms in op-

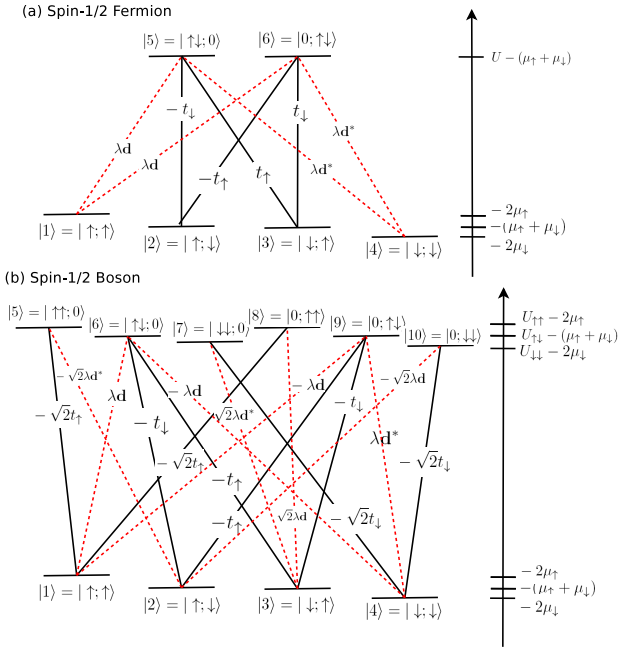

FIG. 1: Transition processes due to spin-conserving tunneling (solid lines) and SO coupling mediated tunneling (dashed lines) for spin-1/2 fermions (a) and spin-1/2 bosons (b). The lowest 4 levels correspond to nearly degenerate ground states. The higher energy levels are the excited states.

tical lattices can be controlled by a Feshbach resonance [24]. To derive the inter-spin interaction in this regime we first consider a two-site tight-binding model,

$$H = -\sum_{\sigma} t_\sigma c^\dagger_{1\sigma} c_{2\sigma} + V_{\rm so} + \frac{1}{2}\sum_{i,\sigma\sigma'} U_{\sigma\sigma'} :n_{i\sigma} n_{i\sigma'}:, \quad (1)$$

where $c^\dagger_{i\sigma}$ creates a particle (either a boson or a fermion) in a Wannier state, $w_{i,\sigma}$, localized at a site i and in a spin state $\sigma \in \{\uparrow,\downarrow\}$. $n_{i\sigma} = c^\dagger_{i\sigma} c_{i\sigma}$ and $U_{\sigma\sigma'} = g_{\sigma\sigma'}\int d\mathbf{x}|w_{i,\sigma}|^2|w_{i,\sigma'}|^2$, where $g_{\sigma\sigma'}$ is the interaction strength between species σ and σ'. Here :: denotes normal ordering. For a general theory the tunneling is assumed to be spin dependent, which is a feature unique to ultracold atom systems [14, 15]. The second term is the SO coupling, which may take various forms depending on the configuration of the laser fields [25]. Here we use the Rashba SO coupling for simplicity,

$$V_{\rm so} = i\lambda c^\dagger_i \mathbf{e}_z \cdot (\sigma \times \mathbf{d}) c_j + \text{h.c.} \quad (2)$$

where $c^\dagger_i = (c^\dagger_{i\uparrow}, c^\dagger_{i\downarrow})$, $\mathbf{d} \equiv (dx, dy)$ is the vector from site j to i, and λ is the SO coupling strength. The magnitude and sign of λ can be tuned in experiments [26] using coherent destructive tunneling methods.

In the deep Mott insulator regime, the effective Hamiltonian can be obtained using the standard Schrieffer-Wolf transformation [14, 27], $H_{\rm eff} = e^{iS} H e^{-iS}$. Let $V = -[iS, H_0]$ to eliminate the first-order term, we have the second order Hamiltonian $H_{\rm eff} = H_0 + \frac{1}{2}[iS, V]$. In the spin representation we define $\mathbf{S}_i = \sum_{ss} c^\dagger_{is}\sigma_{ss'}c_{is'}$, and extend the two-site model to the whole lattice, yielding

$$H_{\rm eff} = \sum_{\langle i,j\rangle}\sum_{\alpha=x,y,z} J_\alpha S^\alpha_i S^\alpha_j + \sum_i \mathbf{B}\cdot\mathbf{S}_i + \sum_{ij}\mathbf{D}_{ij}\cdot(\mathbf{S}_i\times\mathbf{S}_j) + \mathbf{S}_i\cdot\Gamma_{ij}\cdot\mathbf{S}_j. \quad (3)$$

The first two terms denote Heisenberg exchange and Zeeman terms, respectively, while the last two terms arise from SO coupling. In solid state systems the third term is called the DM interaction [28], which is believed to drive multiferroic behavior. In the following we derive the coefficients in the effective Hamiltonian by considering the coupling between four internal degenerate ground states $|\alpha\rangle \in \{|\uparrow;\uparrow\rangle, |\uparrow;\downarrow\rangle, |\downarrow;\uparrow\rangle, |\downarrow;\downarrow\rangle\}$ through the spin independent and dependent tunnelings t_σ and λ. The couplings are different for fermions and bosons, as illustrated in Fig. 1.

Fermionic atoms: For fermionic atoms, there are only two possible excited states $|\text{ex}\rangle = |\uparrow\downarrow;0\rangle$ and $|0;\uparrow\downarrow\rangle$, as shown schematically in Fig. 1 (a). The only relevant two-body interaction is $U_{\uparrow\downarrow} = U$. The couplings between the ground states $|\alpha\rangle$ and the excited state $|\text{ex}\rangle$ are denoted by solid lines for pure spin-conserving tunneling (t_σ terms) and dashed lines for SO coupling mediated tunneling (λ terms). We find $(J_x + J_y)/2 = 4t_\uparrow t_\downarrow/U$, $(J_x - J_y)/2 = 8(-dx^2 + dy^2)U\lambda^2/(U^2 - (\mu_\uparrow - \mu_\downarrow)^2)$, and $J_z = 2(t_\uparrow - t_\downarrow)^2/U - 4d^2U\lambda^2/(U^2 - h^2)$, with $d^2 = dx^2 + dy^2$. The DM interaction coefficient is $\mathbf{D} = 2(t_\uparrow + t_\downarrow)(h^2 - 2U^2)\lambda/(U(h^2 - U^2))(dy, dx, 0)$, and the effective Zeeman field $\mathbf{B} = 4((\mu_\uparrow - \mu_\downarrow) - 2d^2h\lambda^2/(h^2 - U^2))(0, 0, 1)$. Note that without SO coupling the model reduce to the well-known XXZ Heisenberg model with rotation symmetry[13, 14]. However, this symmetry is broken by the SO coupling, yielding an XYZ-type Heisenberg model. Similar results are also observed for bosons.

Bosonic atoms: For bosonic atoms, there are six excited states $|\text{ex}\rangle = |\uparrow\uparrow;0\rangle, |\uparrow\downarrow;0\rangle, |\downarrow\downarrow;0\rangle, |0;\uparrow\uparrow\rangle, |0;\uparrow\downarrow\rangle, |0;\downarrow\downarrow\rangle$, as shown in Fig. 1 (b). Without SO coupling, the only allowed inter-state second-order transition is between $|2\rangle$ and $|3\rangle$, similar to the fermionic case. The presence of SO coupling permits other inter-state transitions, therefore the bosonic case is much more complex than the fermionic case. For simplicity we only show the results for $U_{\uparrow\uparrow} = U_{\downarrow\downarrow} = U_{\uparrow\downarrow} = U$, which yields $(J_x + J_y)/2 = -4t_\uparrow t_\downarrow/U$, $(J_x - J_y)/2 = 4(d_x^2 - d_y^2)U\lambda^2/(U^2 - h^2)$, $J_z = -4t_\uparrow t_\downarrow/U + 2((h^2 - U^2)(t_\uparrow - t_\downarrow)^2 + 2U^2d^2\lambda^2)/U(U^2 - h^2)$, $\mathbf{D} = -2(t_\uparrow + t_\downarrow)(h^2 - 2U^2)\lambda/U(h^2 - U^2)(dx, dy, 0)$, and $\mathbf{B} = (0, 0, 4(\mu_\uparrow - \mu_\downarrow))$.

The last term in Eq. 3 reads as $\mathbf{S}_i\cdot\Gamma_{ij}\cdot\mathbf{S}_j = \eta\frac{8d_xd_yU\lambda^2}{(U^2-h^2)}(S^x_iS^y_j + S^y_jS^x_i)$, where $\eta = +1(-1)$ for fermions (bosons). This term arises from the coupling between states $|1\rangle$ and $|4\rangle$, $|1\rangle\langle 4| = S^x_iS^x_j - S^y_iS^y_j + i(S^x_iS^y_j + S^y_iS^x_j)$.

Here the real part contributes asymmetric terms to the Heisenberg model, while the imaginary part contributes to Γ_{ij}. In a square lattice with $d_x d_y = 0$, this term vanishes. However, for a tilted lattice, such as triangular and honeycomb lattices, this term should be significant.

Lattice parameters: We estimate the possible parameters that can be achieved in a square optical lattice $V(x,y) = V(x)V(y)$, where $V(x) = V_0 \sin^2(k_L x) = sE_R \sin^2(k_L x)$. The recoil energy $E_R = \hbar^2 k_L^2/2m$, where m is the mass of the atom, and k_L is the wavevector of the laser. The SO coupling in free space is $V_{\rm so} = \gamma(p_x\sigma_y - p_y\sigma_x)$, where $\gamma \sim \hbar k_R/m$, k_R is the wavevector of the external Raman lasers, and $k_R \sim k_L$ in most cases. The Raman lasers are pure plane waves, and serve as a perturbation to the hopping between adjacent sites.

We use the Wannier functions of the lowest band without SO coupling to calculate the tight binding parameters: $t = \int dx w_i^*(x)[p^2/2m + V(x)]w_{i+1}(x)$ and $\lambda = \int dx w_i^*(x) V_{\rm so} w_{i+1}(x)$. In a square lattice, coordinates decouple and the Bloch functions are Mathieu functions. The Wannier functions can be obtained from the Fourier transformation of the Bloch functions. Our numerical results are presented in Fig. 2 (a). The large s limit, $t \sim t_{\rm appr.} = 4E_R/\sqrt{\pi}s^{3/4}\exp(-2\sqrt{s})$, is also plotted for comparison. Note that $U/E_R \sim (8/\pi)^{1/2} k a_s s^{3/4}$ is in general much larger than t and can be controlled through Feshbach resonance independently.

In Fig. 2 (b) we plot $|\mathbf{D}|/|\mathbf{J}|$ as a function of $\xi = \lambda/t$ for $U_{\sigma\sigma'} = U$, $t_\sigma = t$. $|\mathbf{D}|/|\mathbf{J}|$ reaches the maximum value of 1.0 at $\lambda = t$. This is in sharp contrast to models of weak multiferroic effects in solids with $D/J \sim 0.001-0.1$, which is generally induced by small atomic displacements [29]. Optical lattices, by contrast, can be tuned to exhibit either weak or strong DM terms. This enhanced tunability enables optical lattice systems to single out the effects of strong DM interactions and study the impact of the DM term.

There are notable differences between our model and

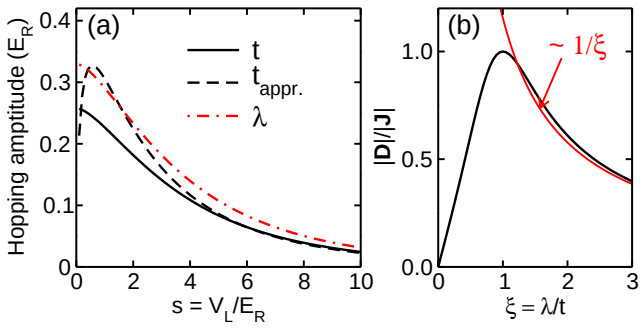

FIG. 2: (Color online). (a) Tunneling amplitudes as a function of lattice depth. t is the hopping due to the kinetic energy, $t_{\rm appr.}$ is the analytical expression in the deep lattice regime, and λ is the SO mediated hopping strength. (b) Plot of $|\mathbf{D}|/|\mathbf{J}|$ as a function of λ/t for $U_{\sigma\sigma'} = U$, $t_\sigma = t$.

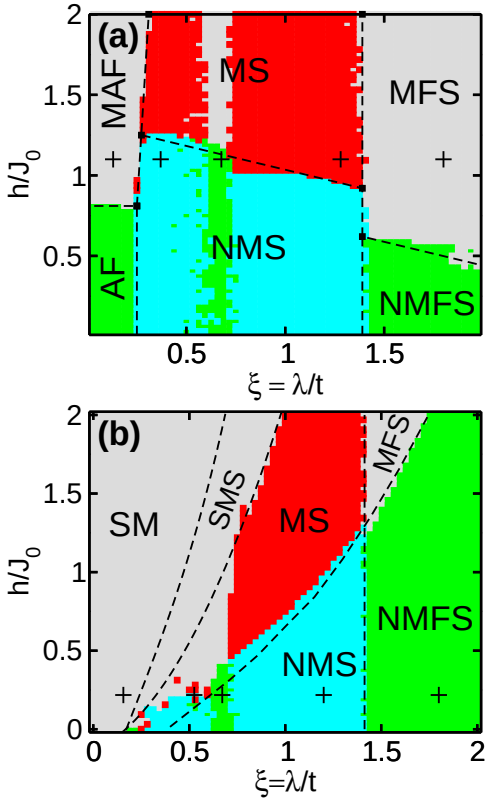

FIG. 3: Phase diagrams of 2D optical lattices with fermions (a) and bosons (b) obtained from classical Monte Carlo simulations for an 8×8 lattice at temperature $T = 0.05J_0$. The phases diagrams are determined by the magnetization order, the spiral order, and the spin structure factor. Different regions correspond to: $M = 0$, $P = 0$ for green, $M \neq 0$, $P = 0$ for grey, $M = 0, P \neq 0$ for cyan, and $M \neq 0$, $P \neq 0$ for red. The abbreviations are: (a) AF: antiferromagnetic phase with zero total magnetization; MAF: antiferromagnetic phase with non-zero total magnetization; NS: zero magnetization spiral order; MS: magnetic spiral order; NMFS: nonmagnetic flux spiral phase; MFS: magnetic flux spiral phase. In (b), SM: simply magnetic order; SMS: simply magnetic spiral order: Other abbreviations are the same as in (a). The dashed lines are guides to the eye. The spin structure factors of the points marked by plus signs are shown in Fig. 4.

corresponding models of solids (i) In solids the SO coupling arises from intrinsic (atomic) SO coupling and $\mathbf{D}$ is generally along the z direction (out of plane). However, in our model $\mathbf{D}$ is in the plane and the out of plane component is zero. (ii) In our effective spin model, J_{ij}^α depends on the direction of the bond (d_x, d_y) and the SO coupling strength, while in solids J_{ij}^α is independent of SO coupling due to its negligible roles.

Spiral Order and Multiferroics in 2D Optical Lattices: We explore the rich phase diagrams of the effective spin Hamiltonian using classical MC simulations. The classical MC has been widely used to explore the phase diagrams of the Heisenberg model with DM interactions in the context of solids [8, 30–32] (and hence weak DM in-

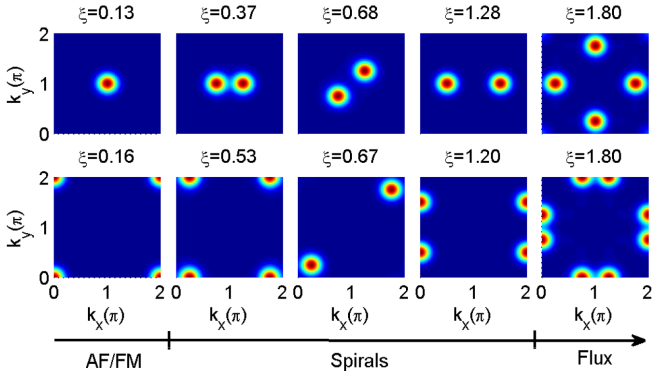

FIG. 4: Spin structure factors for different quantum phases marked by plus sign in Fig. 3. The upper panels show the results for fermion at $h/J_0 = 1.1$, while the lower panels show the results for boson at $h/J_0 = 0.218$.

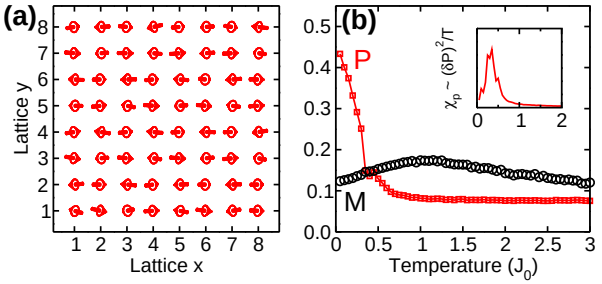

FIG. 5: (a) The spin configuration of fermions in an 8×8 lattice at $T = 0.05J_0$, $\xi = 1.0$ and $h/J_0 = 1.5$. The corresponding magnetization and spiral order as a function of temperature is shown in (b), with the inset plot $\chi_p \sim (\delta P)^2/T$ vs temperature, which indicates a phase transition at $T_c \sim 0.5J_0$. Similar features can also been found for bosons with the same parameters.

teractions). This method may not be used to determine the precise boundaries between different phases but can be an efficient tool to determine different possible phases. Due to the unique features of our effective model (e.g., strong DM interactions) the phase diagrams we present here are much more rich and comprehensive than those explored in the context of solids. We focus on the regime where $t_\sigma = t$ and $U_{\sigma\sigma'} = U$ (spin independent), and define $J_0 = 4t^2/U$ as the energy scale. The rescaled effective Hamiltonian becomes

$$H = \eta \sum_{ij} \sum_{a=x,y,z} j^a S_i^a S_j^a + \mathbf{D} \cdot \mathbf{S}_i \times \mathbf{S}_j + h \sum_i S_i^z, \quad (4)$$

where $j^x = -1 + (d_x^2 - d_y^2)\xi^2$, $j_y = -1 - (d_x^2 - d_y^2)\xi^2$, $j_z = -1 + \xi^2$, $\mathbf{D} = -2\xi(d_y, d_x, 0)$, and $\xi = \lambda/J_0$.

Eq. 4 hosts a variety of magnetic and spin spiral phases, which are generally characterized by the magnetic and spiral order parameters[33, 34]

$$M = \sum_i S_i^z \text{ and } \quad \mathbf{P} = \sum_{\langle i,j \rangle} \mathbf{d}_{ij} \times \mathbf{S}_i \times \mathbf{S}_j. \quad (5)$$

However, these two order parameters do not fully characterize the phase diagrams because in some cases there are still local magnetic or spiral orders although both M and $|P|$ are vanishingly small. In these cases, we also take into account the spin structure factor:

$$S(\mathbf{k}) = \sum_{i,j} \langle \mathbf{S}_i \cdot \mathbf{S}_j \rangle \exp(i\mathbf{k} \cdot (\mathbf{R}_i - \mathbf{R}_j)), \quad (6)$$

which shows peaks at different position in momentum space for different phases. For instance, the peak of the spin structure factor is at $\mathbf{k} = (0, 0)$ for ferromagnetic phases, $\mathbf{k} = (\pi, \pi)$ for antiferromagnetic phases, and $(\pi, 0)$ (or $(0, \pi)$) for the flux spiral phase ($P = 0$ but with nontrivial local spin structure). General spiral orders correspond to other k. We obtain the phase diagrams by analyzing both the order parameters and spin structure factors. We have not checked for long range order in the spin structure factor. We expect quasi-long range order to accompany magnetized phases at low h, e.g., a ferromagnetic phase for $\xi \ll 1$.

Fig. 3 shows the phase diagrams of an 8×8 lattice for both fermions and bosons. The results are obtained after 10^6 thermalization steps followed by 10^6 sampling steps in each MC run at low temperature ($T = 0.05J_0$). We have checked that for lower temperatures the phase diagrams do not change quantitatively. We also verify that similar phase diagrams can be obtained for larger system sizes, however, the spiral orders in larger optical lattice become more complicated, and the boundary between different quantum phases is shifted.

The phase diagrams show a rich interplay between magnetic orders and spin spiral orders. For instance, for fermions with small SO coupling ($\xi < 0.25$), the ground states are anti-ferromagnetic states with zero (nonzero) magnetization for a Zeeman field $h/J_0 < 0.8$ ($h/J_0 > 0.8$). While for large SO coupling ($\xi > 1.45$), the ground states are either nonmagnetic or magnetic flux spiral phases (similar to the flux phase with a small spiral order P). For $\xi \gg 1$ the DM term is not important because $D/J \sim 1/\xi$, therefore the pure flux phase with zero spiral order can be observed. Similarly, the increasing SO coupling for bosonic atoms gives rise to a series of transitions from simply magnetic (ferromagnetic at small h) order to simply magnetic spiral order (with zero total spiral order but local spiral structure), then to magnetic spiral orders (or non-magnetic spiral orders) and finally to flux spiral orders. The emergence of the spiral order and flux order with increasing SOC can be clearly seen from the change of the spin structure factors in Fig. 4, which shift from $\mathbf{k} = (0, 0)$ or (π, π) to $(\pi, 0)$ and $(0, \pi)$.

The spin spiral order phase transition temperature is comparable to the magnetic phase transition temperature, $\sim J_0$. In Fig. 5 (a), we plot the spin configuration of fermions at $T = 0.05J_0$, $\xi = 1.0$ and $h = 1.5$

(MS phase), which show clear spiral ordering. The corresponding order parameters P and M are plotted in Fig. 5 (b) as a function of temperature. The inset show susceptibility $\chi_p \sim (\delta P)^2/T$. We see a phase transition at $T_c \sim 0.5J_0$, which is comparable to the magnetic critical temperature [14] (in 2D, the Heisenberg model has a critical temperature $T_c = J_0$ in mean-field theory). Note that spiral order can also exist in the frustrated model without SO coupling, however, the critical temperature is generally much smaller than the magnetic phase transition temperature [8, 35]. Our results therefore show that SO coupling in the absence of frustration provides an excellent platform for searching for high-T_c spiral orders and multiferroics in optical lattices.

Finally we note that different spiral orders may be observed using the optical Bragg scattering methods [36], which probe different spin structure factors for different spiral orders. Similar methods have been widely used in solid state systems. Furthermore, in optical lattices, the local spin magnetization at each lattice site (thus the magnetic order M) as well as the local spin-spin correlations (thus the spiral order P) can be measured directly [37, 38], which provides a powerful new tool for understanding the physics of spiral orders and multiferroic effects in optical lattices.

Note Added. During the preparation of this manuscript we became aware of preprints [39–41] on similar topics.

Acknowledgement MG thanks S. Liang for numerical assistance with classical MC simulations. This work is supported by AFOSR (FA9550-11-1-0313), DARPA-YFA (N66001-10-1-4025, N66001-11-1-4122), ARO (W911NF-09-1-0248), NSF-PHY (1104546), and the Jeffress Memorial Trust (J-992).

* Email: chuanwei.zhang@utdallas.edu

[1] M. Fiebig, J. Phys. D: Appl. Phys. **38**, R123 (2005);M. Dawber, K. M. Rabe, and J. F. Scott Rev. Mod. Phys. **77**, 1083 (2005); D. N. Basov *et al.* Rev. Mod. Phys. **83**, 471 (2011); G. Catalan *et al.*, Rev. Mod. Phys. **84**, 119 (2012).
[2] Y. Tokura and S. Seki, Adv. Mater. **22**, 1554 (2010).
[3] T. Kimura, Annu. Rev. Mater. Res. **37**, 387-413 (2007).
[4] S.-W. Cheong and M. Mostovoy, Nature Materials **6**, 13 (2007).
[5] R. Ramesh and N. A. Spaldin, Nature Materials **6**, 21 (2007).
[6] W. Eerenstein, N. D. Mathur, and J. F. Scott, Nature **442**, 759 (2006).
[7] Y. Tokura, Science **312**, 1481 (2006).
[8] G. Jin, K. Cao, G.-C. Guo, and L. He, Phys. Rev. Lett. **108**, 187205 (2012).
[9] I. A. Sergienko and E. Dagotto, Phys. Rev. B **73**, 094434 (2006).
[10] H. Katsura, N. Nagoasa and A. V. Balatsky, Rev. Mod. Phys. **95**, 057205 (2005).
[11] M. Greiner et al, Nature (London) **415**, 39 (2002).
[12] I. Bloch, J. Dalibard, and W. Zwerger, Rev. Mod. Phys. **80**, 885 (2008).
[13] A. B. Kuklov and B. V. Svistunov, Phys. Rev. Lett. **90**, 100401 (2003).
[14] L. -M. Duan, E. Demler and M. D. Lukin, Phys. Rev. Lett. **91**, 090402 (2003).
[15] E. Altman, W. Hofstetter, E. Demler and M. D. Lukin, New Journal of Physics **5**, 113, (2003).
[16] S. Trotzky, P. Cheinet, S. Fölling, M. Feld, U. Schnorrberger, A. M. Rey, A. Polkovnikov, E. A. Demler, M. D. Lukin and I. Bloch, Science **319**, 295 (2008).
[17] J. Struck, C. Ölschläger, R. Le Targat, P. Soltan-Panahi, A. Eckardt, M. Lewenstein, P. Windpassinger and K. Sengstock, Science **333**, 996 (2011).
[18] Y.-J. Lin, K. Jimenez-Garcia, and I. B. Spielman, Nature **471**, 83 (2011).
[19] S. Chen, J.-Y. Zhang, S.-C. Ji, Z. Chen, L. Zhang, Z.-D. Du, Y. Deng, H. Zhai, J.-W. Pan, arXiv:1201.6018.
[20] Z. Fu, P. Wang, S. Chai, L. Huang, J. Zhang, Phys. Rev. A **84**, 043609 (2011).
[21] P. Wang, Z.-Q. Yu, Z. Fu, J. Miao, L. Huang, S. Chai, H. Zhai, J. Zhang, arXiv:1204.1887.
[22] Y. Zhang, and C. Zhang, arXiv:1203.2389.
[23] L. W. Cheuk, A. T. Sommer, Z. Hadzibabic, T. Yefsah, W. S. Bakr, M. W. Zwierlein, arXiv:1205.3483.
[24] M. Köhl et al, Rev. Mod. Phys. **94**, 080403 (2005).
[25] Y. Zhang and C. Zhang, Phys. Rev. Lett. **108**, 035302 (2012).
[26] Y. Zhang, G. Chen, C. Zhang, arXiv:1111.4778.
[27] A. C. Hewson, The Kondo Problems to Heavy Fermions (Cambridge University Press, Cambridge, England, 1997).
[28] I. E. Dzyaloshinskii, Sov. Phys. JETP **19**, 960 (1964). T. Moriya, Phys. Rev. **120**, 91 (1960).
[29] I. A. Sergienko and E. Dagotto, Phys. Rev. B 73, 094434 (2006).
[30] C. Sen, S. Liang, and E. Dagotto, Phys. Rev. B 85, 174418 (2012).
[31] S. Liang, M. Daghofer, S. Dong, C. Sen, and E. Dagotto, Phys. Rev. B **84**, 024408 (2011).
[32] S. Dong, K. Yamauchi, S. Yunoki, R. Yu, S. Liang, A. Moreo, J.-M. Liu, S. Picozzi, and E. Dagotto, Phys. Rev. Lett. **103**, 127201 (2009).
[33] M. Mostovoy, Phys. Rev. Lett. **96**, 067601 (2006).
[34] H. Katsura, N. Nagaosa, and A. Balatsky, Phys. Rev. Lett. **95**, 057205 (2005).
[35] G. R. Blake, L. C. Chapon, P. G. Radaelli, S. Park, N. Hur, S-W. Cheong, and J. Rodríguez-Carvaja, Phys. Rev. B **71**, 214402 (2005).
[36] T. A. Corcovilos, S. K. Baur, J. M. Hitchcock, E. J. Mueller, and R. G. Hulet, Phys. Rev. A **81**, 013415 (2010).
[37] W. S. Bakr, J. I. Gillen, A. Peng, S. Fölling, and M. Greiner, Nature 462, 74 (2009).
[38] C. Weitenberg, M. Endres, J. F. Sherson, M. Cheneau, P. Schauβ, T. Fukuhara, I. Bloch, and S. Kuhr, Nature **471**, 319 (2011).
[39] J. Radic, A. Di Ciolo, K. Sun, V. Galitski, arXiv:1205.2110.
[40] W. S. Cole, S. Z. Zhang, A. Paramekanti, and N Trivedi, arXiv:1205.2319.
[41] Z. Cai, X. Zhou, C. Wu, arXiv:1205.3116.